Visual physiology of the lateral geniculate nucleus in two species of New World monkey: *Saimiri sciureus* and *Aotus trivirgatis*

W. Martin Usrey and R. Clay Reid

Department of Neurobiology, Harvard Medical School, 220 Longwood Avenue, Boston, MA 02115, USA

(Received 22 September 1999; accepted after revision 18 November 1999)

1. Visual responses were recorded from neurones in the magnocellular and parvocellular layers of the lateral geniculate nucleus (LGN) of the thalamus in two species of New World monkeys – the diurnal squirrel monkey (*Saimiri sciureus*) and the nocturnal owl monkey (*Aotus trivirgatis*). Recording sites were reconstructed in postmortem tissue and comparisons were made between the response properties of magnocellular and parvocellular neurones.

2. Receptive fields were characterized with both white noise and drifting gratings. We found that most of the differences between magnocellular and parvocellular neurones that have been described in the macaque monkey hold for the squirrel monkey and owl monkey. In squirrel monkey and owl monkey, receptive fields of magnocellular neurones were larger than those of parvocellular neurones at similar eccentricities. Although visual responses in the owl monkey were significantly slower than in the squirrel monkey, in both species magnocellular neurones differed from parvocellular neurones in that their responses (1) had higher contrast gains, (2) tended to peak at higher temporal frequencies (but with considerable overlap), (3) had shorter response latencies, and (4) were more transient.

3. The strength of a neurone's receptive-field surround was assessed by comparing neuronal responses to gratings of optimal spatial frequency with responses to gratings of low spatial frequency. Using this approach, receptive-field surrounds were found to be equally strong on average for magnocellular and parvocellular neurones.

4. Spatial summation, as measured by a null test, was linear for all magnocellular and parvocellular cells tested; that is, Y cells were not observed in either species. Finally, most magnocellular neurones showed a contrast gain control mechanism, although this was not seen for parvocellular neurones.

In the mammalian nervous system, sensory information is processed and conveyed from one level to the next via parallel pathways. In the visual system of primates, these parallel pathways are exceptionally distinct at the level of the lateral geniculate nucleus (LGN) of the thalamus. Neurones in the magnocellular, parvocellular and koniocellular layers of the LGN receive input from different classes of retinal ganglion cells, give rise to axons that target different layers of primary visual cortex, and differ in their visual response properties (reviewed in Schiller & Logothetis, 1990; Shapley, 1992; Merigan & Maunsell, 1993; Casagrande, 1994; Casagrande & Kaas, 1994; Hendry & Reid, 2000).

Much of our understanding of visual physiology in the primate retina and LGN comes from studies of the macaque monkey (De Valois, 1960; Wiesel & Hubel, 1966; Gouras, 1968; De Monasterio & Gouras, 1975; Schiller & Malpeli, 1978; Kaplan & Shapley, 1982, 1986; Derrington & Lennie, 1984; Derrington *et al.* 1984; Benardete *et al.* 1992; Reid & Shapley, 1992; Maunsell *et al.* 1999; reviewed in Lee, 1996). Compared with parvocellular neurones, magnocellular neurones and their retinal inputs have larger receptive fields, respond better to low contrast stimuli, are somewhat more sensitive to quickly moving stimuli or are modulated at high temporal frequency (but see Hawken *et al.* 1996), and respond with a shorter latency following the presentation of a visual stimulus. Magnocellular neurones have little selectivity for colour, while most parvocellular neurones are colour-selective, particularly red/green opponent. Finally, some magnocellular-projecting retinal ganglion cells have a contrast gain control mechanism similar to that described in the cat retina (Shapley & Victor, 1978).

Although it has been assumed that differences between magnocellular and parvocellular neurones are common to all primates, few studies have examined the extent to which these differences are seen in two commonly studied species of New World monkeys – the squirrel monkey (*Saimiri*

sciureus) and the owl monkey (*Aotus trivirgatis*). Most studies of the LGN of these species have concentrated on anatomical organization, pattern of retinal inputs (eye specificity and retinotopy), and receptive-field size (Doty *et al.* 1966; Jones, 1966; Kaas *et al.* 1972, 1978; Fitzpatrick *et al.* 1983; Diamond *et al.* 1985). A recent study by O'Keefe and colleagues (1998; see also Sherman *et al.* 1976) presents a more thorough analysis of the physiological differences between magnocellular and parvocellular neurones in the nocturnal owl monkey. To our knowledge, comparable work has not been performed for the squirrel monkey (although the squirrel monkey LGN has been examined for colour opponency: Jacobs & De Valois, 1965; Jacobs, 1984). Given the large literature of anatomy and visual physiology of the striate and extrastriate cortex of squirrel monkeys and owl monkeys (reviewed in Casagrande & Kaas, 1994), a more thorough survey of geniculate responses in these animals is needed.

METHODS

Animal preparation

All surgical and experimental procedures conformed to National Institutes of Health and US Department of Agriculture guidelines and were carried out with the approval of the Harvard Medical Area Standing Committee on Animals. Four adult male squirrel monkeys (*Saimiri sciureus*) and four adult owl monkeys (*Aotus trivirgatis*), both male and female, were used in this study. Surgical anaesthesia was induced with ketamine (10 mg kg^{-1} I.M.; supplemented as needed in amounts of 5 mg kg^{-1}). A tracheotomy was performed and animals were placed in a stereotaxic apparatus where anaesthesia was maintained with 1·5–2·5% isoflurane in nitrous oxide and oxygen (1:1). If there was any indication that the animal was not adequately anaesthetized, the percentage of isoflurane delivered to the animal was increased (in 0·5% increments). Body temperature was maintained at 37 °C using a thermostatically controlled heating blanket. Temperature, ECG, EEG and expired CO_2 were monitored continuously throughout the experiment. Pupils were dilated with 1% atropine sulphate, and eyes were fitted with appropriate contact lenses and focused on a tangent screen located 172 cm in front of the animal. A midline scalp incision was made and a small craniotomy was made above the LGN. All wound margins were infused with lidocaine.

Once all surgical procedures were complete, animals were paralysed with vecuronium bromide (0·2 mg kg^{-1} h^{-1} I.V.) and ventilated mechanically. Proper depth of anaesthesia was ensured throughout the experiment by (1) monitoring the EEG for changes in slow-wave/spindle activity, and (2) monitoring the ECG and expired CO_2 for changes associated with a decrease in the depth of anaesthesia. If any of these measures indicated that the animal was not properly anaesthetized, the percentage of isoflurane delivered to the animal was increased in 0·5% increments. In some animals, the paralytic agent was withdrawn in order to test whether the above criteria adequately indicated the depth of anaesthesia.

At the end of each experiment, animals were given a lethal overdose of sodium thiopental (100 mg kg^{-1}). Once the EEG, heart rate and CO_2 levels indicated that the animal had expired, animals were perfused through the heart with saline followed by 4% paraformaldehyde in 0·1 M phosphate buffer. After fixation, brains were rinsed in a 10% solution of sucrose in phosphate buffer and immersed overnight in a 20% solution of sucrose in phosphate buffer. Brains were sectioned coronally at 50 μm on a freezing microtome. Sections containing the LGN were mounted onto gelatin-subbed slides, counterstained with thionin, dehydrated with alcohol, cleared with xylene, and coverslipped in permount. Electrode tracks, lesions (made during the experiment by passing 4 μA current for 4 s) and recording sites were reconstructed using a Zeiss microscope equipped with the Neurolucida reconstruction system (MicroBrightField, Inc; Colchester, VT, USA). Reconstruction of electrode tracks was usually based on two or more lesions along the track. In cases where only a single lesion was made, reconstructions were based on documenting the depth of the lesion and the depth of the surface of the LGN (as indicated by the first visual neurone encountered).

Electrophysiological recordings and visual stimuli

Recordings were made from neurones in the LGN with tungsten in glass electrodes (Alan Ainsworth, London). Spike times and waveforms were recorded to disk (with 100 μs resolution) by a PC running the Discovery software package (Datawave Technologies, Longmont, CO, USA). Spike isolation was confirmed with off-line waveform analysis and by the presence of a refractory period, as seen in the autocorrelograms.

Receptive fields of geniculate neurones were mapped quantitatively by reverse correlation using pseudorandom spatiotemporal white-noise stimuli (m-sequences; Sutter, 1992; Reid *et al.* 1997). The stimuli were created with an AT-Vista graphics card (Truevision, Indianapolis, IN, USA) running at a frame rate of 128 Hz. The stimulus program was developed with subroutines from a runtime library, YARL, written by Karl Gegenfurtner (New York University). The mean luminance of the stimulus monitor was 40–50 cd m^{-2}.

The white-noise stimulus consisted of a 16×16 grid of squares (pixels) that were white or black one-half of the time, as determined by an m-sequence of length $2^{15} - 1$. The stimulus was updated either every frame of the display (7·8 ms) or every other frame (15·6 ms). The entire sequence (~4 or 8 min) was often repeated several times. The size of individual pixels varied (from 0·075 to 0·6 deg on a side) depending on the receptive fields under study, which were between 5 and 25 deg eccentric. In most cases 8–16 pixels filled the receptive-field centre.

In many cases, sinusoidal grating stimuli were also used to characterize the neurones under study. Responses to gratings (the first Fourier coefficient, or f1) drifting at 4 Hz were studied at a range of spatial frequencies. Next, the peak spatial frequency was used to study the responses at a range of contrasts (1·5–100%) and a range of temporal frequencies (0·5–32 Hz, occasionally as high as 64 Hz). Finally, for most neurones, classification of X cells *versus* Y cells was determined with a modified null test, performed with contrast-reversing gratings at several spatial frequencies including the peak spatial frequency, and 2 and 4 times the peak spatial frequency (Enroth-Cugell & Robson, 1966; Hochstein & Shapley, 1976).

Receptive-field mapping: reverse correlation

Spatiotemporal receptive-field maps (kernels) were calculated from the responses to the white-noise (m-sequence) stimulus by a reverse-correlation method (Sutter, 1992; Reid *et al.* 1997). For each delay between stimulus and response and for each of the 16×16 pixels, we calculated the average stimulus that preceded each spike (+1 for white, −1 for black). For each of the pixels, the kernel can also be thought of as the average firing rate of the neurone, above or below the mean, following the bright phase of the stimulus at that

pixel (the impulse response). When normalized by the product of the bin width and the total duration of the stimulus, the result is expressed in units of spikes per second.

In order to assess the time course and magnitudes of the response, it was necessary to identify the pixels in the receptive-field centre. First, the largest single response was located: the position of greatest sensitivity at the most effective delay between stimulus and response. Next, the spatial receptive field was averaged over a range of times (31·2 ms total, or 4 display frames) before and after the best delay, to define the spatial receptive field. The centre pixels were defined as all contiguous spatial positions in this spatial receptive field that were the same sign as the strongest response and were greater than two standard deviations above the baseline noise. The baseline noise was taken as the standard deviation of the kernel values for all pixels and for delays (54·4–108·7 ms) that were well beyond the peak response. The impulse responses of all of the pixels in the centre were added together to yield the centre impulse response.

Parameters quantifying the impulse responses were calculated as follows (see Fig. 5*A*). The time of maximum response, t_{max}, was calculated from the centre impulse response, sampled in 1·9 ms bins. The rebound time, $t_{rebound}$, was defined as the first time, following t_{max}, that the response was opposite in sign from the maximum response. The peak magnitude, which quantifies the first phase of the response, the response before the rebound, was defined as the integral of the impulse response for all times before $t_{rebound}$. Finally, the rebound magnitude was defined as the integral of the impulse response for times greater than $t_{rebound}$ (up to 233 ms).

The size of receptive-field centres was quantified by fitting the best single two-dimensional Gaussian to the spatial receptive field (as defined above) using the expression $A\exp(-|x - x_c|^2/\sigma^2)$, where A is the amplitude, x_c the centre, and σ the standard deviation of the Gaussian fit, in degrees. Empirically, we have found that a circle of radius $1{\cdot}75\sigma$ corresponds well to the spatial extent of the receptive field centre, that is, the border between the centre and the surround (see Usrey *et al.* 1999). For this reason, we report the size of the receptive fields (see Fig. 4, below) to be $3{\cdot}5\sigma$.

RESULTS

We studied the physiological properties of 23 magnocellular and 54 parvocellular neurones in four squirrel monkeys and

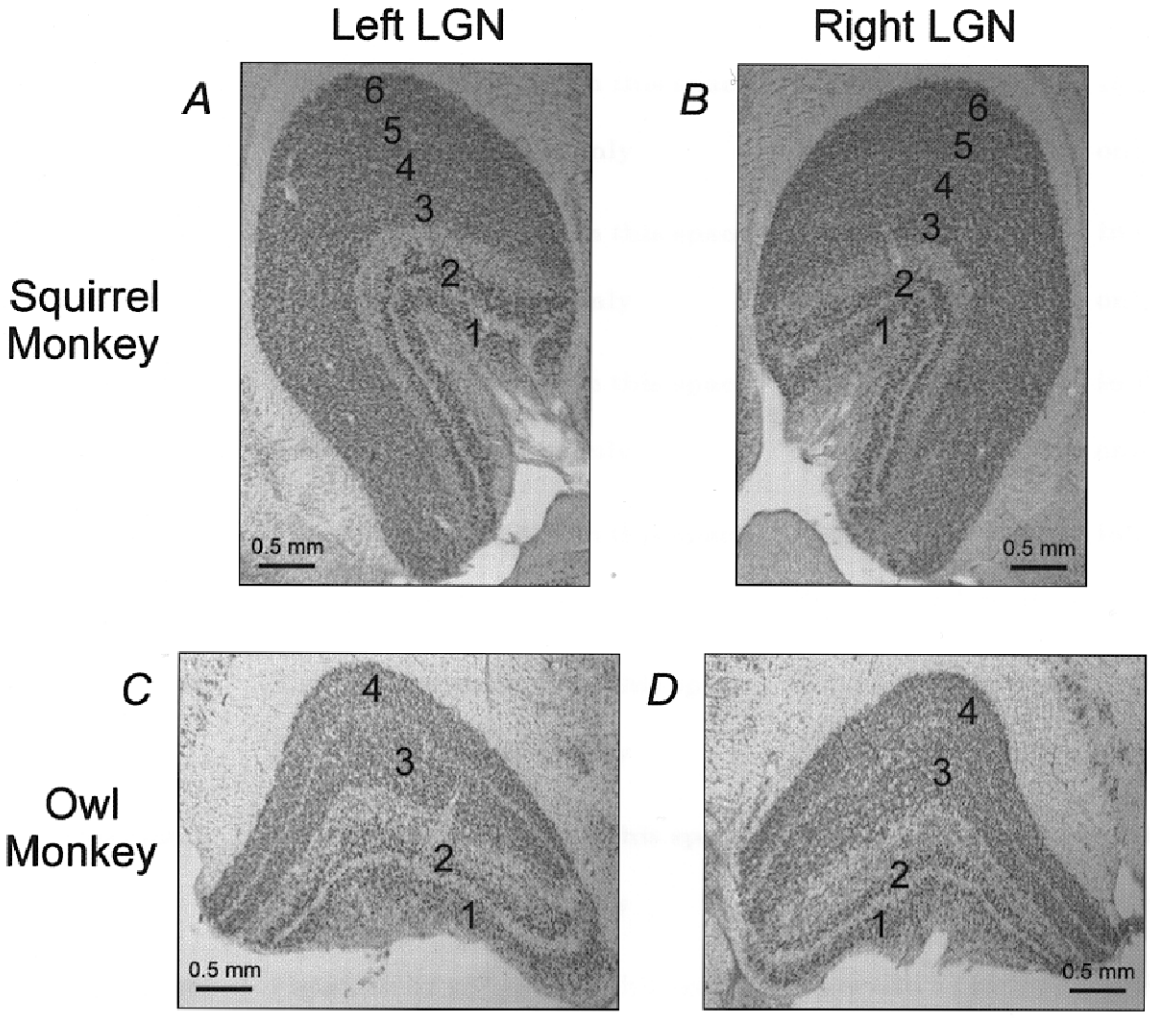

Figure 1. Nissl-stained sections of squirrel monkey LGN and owl monkey LGN

In the squirrel monkey (*A* and *B*), the LGN contains two magnocellular layers (layers 1 and 2) and 4 parvocellular layers (layers 3, 4, 5, and 6). In the owl monkey (*C* and *D*), the LGN contains two magnocellular layers (layers 1 and 2) and two parvocellular layers (layers 3 and 4).

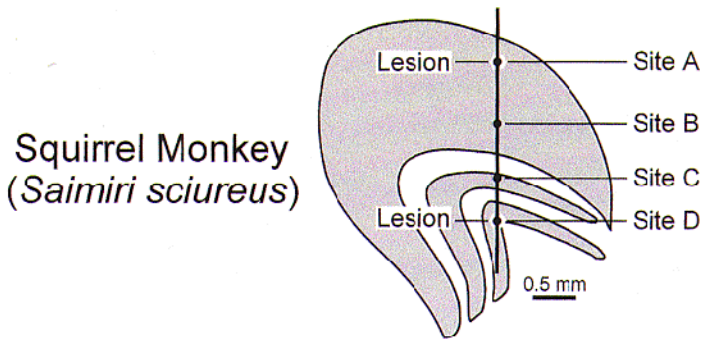
Squirrel Monkey
(Saimiri sciureus)
Lesion
Site A
Site B
Site C
Lesion
Site D
0.5 mm

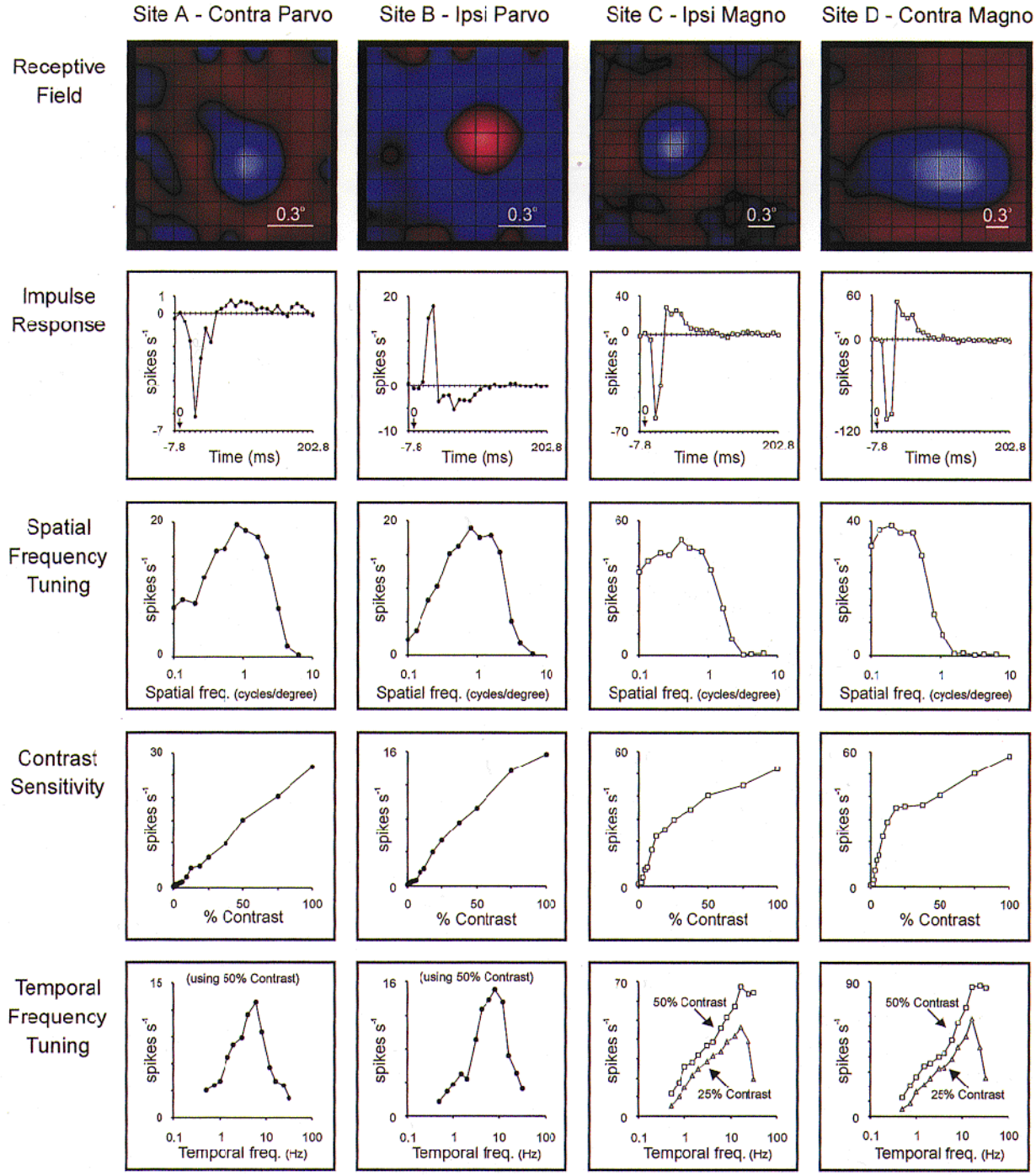
Site A - Contra Parvo
Site B - Ipsi Parvo
Site C - Ipsi Magno
Site D - Contra Magno
Receptive Field
Impulse Response
Spatial Frequency Tuning
Contrast Sensitivity
Temporal Frequency Tuning
0.3°
spikes s⁻¹
Time (ms)
-7.8
202.8
Spatial freq. (cycles/degree)
% Contrast
(using 50% Contrast)
50% Contrast
25% Contrast
Temporal freq. (Hz)

of 31 magnocellular and 34 parvocellular neurones in four owl monkeys. Assignment of these neurones to either magnocellular or parvocellular layers was determined as outlined below.

In squirrel monkeys and owl monkeys, the LGN is a multilayered structure (Fig. 1). In both species, magnocellular layers 1 and 2 are ventral to the parvocellular layers and receive input from the contralateral and ipsilateral eyes, respectively. Squirrel monkeys and owl monkeys differ in their number of parvocellular layers. In the owl monkey, an intercalated (or koniocellular) layer separates parvocellular layers 3 and 4. Layer 3 receives input from the ipsilateral eye, layer 4 from the contralateral eye. In the squirrel monkey, the parvocellular layers are not distinct from each other in Nissl-stained tissue. Nevertheless, injections of anterograde tracer into the eye of the squirrel monkey suggest that there are 4 parvocellular layers – layers 3, 4, 5 and 6 – that receive input from the ipsi-, contra-, ipsi- and contralateral eyes, respectively (Fitzpatrick *et al.* 1983). It should be noted, however, that layers 3 and 4, and 4 and 5 often interdigitate in the squirrel monkey (D. Fitzpatrick, personal communication).

During a typical electrode penetration (Figs 2 and 3), the location of the electrode within the LGN was clear. When passing between parvocellular layers or between magnocellular layers, the shift in ocular dominance provided strong evidence of the location of the electrode. Most important to this study, however, was knowing when the electrode exited the parvocellular layers and entered the underlying magnocellular layers. In both squirrel monkeys and owl monkeys, the thick koniocellular layer that separates parvocellular layer 3 and magnocellular layer 2 (see Fig. 1) serves as a useful landmark. Upon entering this koniocellular layer, there is a dramatic decrease in background neural activity. With further progression of the electrode, there is a tremendous increase in background activity as the electrode enters magnocellular layer 2. While all of these criteria were useful for guiding the collection of data during an experiment, the location of recording sites was confirmed from the location of lesions and the reconstruction of electrode tracts in postmortem tissue (see Methods). The location of most neurones was confirmed histologically; in no case was there a mismatch between the histology and the physiologically predicted location of the recording site.

For neurones in each layer, we examined their visual responses with a variety of stimulus protocols. Examples from each of the four layers are illustrated in Fig. 2 for the squirrel monkey and Fig. 3 for the owl monkey. For all neurones in this study, receptive fields were first mapped by reverse correlation with a white-noise (m-sequence) stimulus (Sutter, 1992; Reid *et al.* 1997). This procedure yielded a detailed characterization of the receptive field, both in space and in time. Spatial receptive fields of neurones in each layer of the LGN are shown in the top row of panels in Figs 2 and 3 (on-responses indicated in red, off-responses in blue). These plots are useful for illustrating the centre/surround organization of the receptive fields, but they give no information about the temporal aspects of the visual responses.

The time course of the visual response – the impulse response (see Methods) – is shown below each of the spatial receptive fields (Figs 2 and 3). These curves can be thought of as the average response, or the deviation from the mean rate, evoked by the bright phase of the stimulus at time zero. The impulse responses shown were summed over all of the pixels in the receptive-field centre. Because the stimulus was binary – that is, if a pixel was not light, it was necessarily dark – a negative response to the bright stimulus (seen for off-centre neurones) is formally equivalent to a positive response to the *dark* phase of the stimulus. In the squirrel monkey, a typical impulse response reaches its peak at approximately 20–30 ms following the stimulus (Fig. 2, second row); for owl monkeys peaks are at approximately 30–45 ms (Fig. 3, second row). Following the peak, the response decays and there is an overshoot, or rebound. At long delays, the visual stimulus no longer has an influence on the activity of the neurone and the impulse–response curve returns to zero. Several points can be appreciated from the impulse responses: compared with parvocellular neurones, magnocellular neurones tend to have responses that are slightly faster, greater in magnitude, and with more pronounced rebounds.

Once neurones were mapped with white noise, they were studied with drifting gratings. In most cases, spatial

Figure 2. Examples of the response properties of neurones encountered during a typical electrode penetration across the depth of the LGN in the squirrel monkey

A reconstruction of the electrode tract and recording sites is shown at the top of Fig. 2. Neurones were recorded in four different layers (sites A–D, top of figure). Abbreviations: Contra, contralateral; Ipsi, ipsilateral; Magno, magnocellular neurone; Parvo, parvocellular neurone. The receptive fields of each of the four neurones are shown in the top row of panels. Receptive fields were mapped using a spatiotemporal white-noise stimulus (see Methods). The squares in the grid overlay correspond to the pixels in the stimulus. On-responses are shown in red, off-responses in blue. The greater the response, the brighter the pixel. Receptive fields are shown smoothed by $\frac{1}{2}$ pixel. Shown below each receptive field are plots of the neurone's time course of response (impulse response), spatial frequency tuning, contrast gain and temporal-frequency tuning (see Methods).

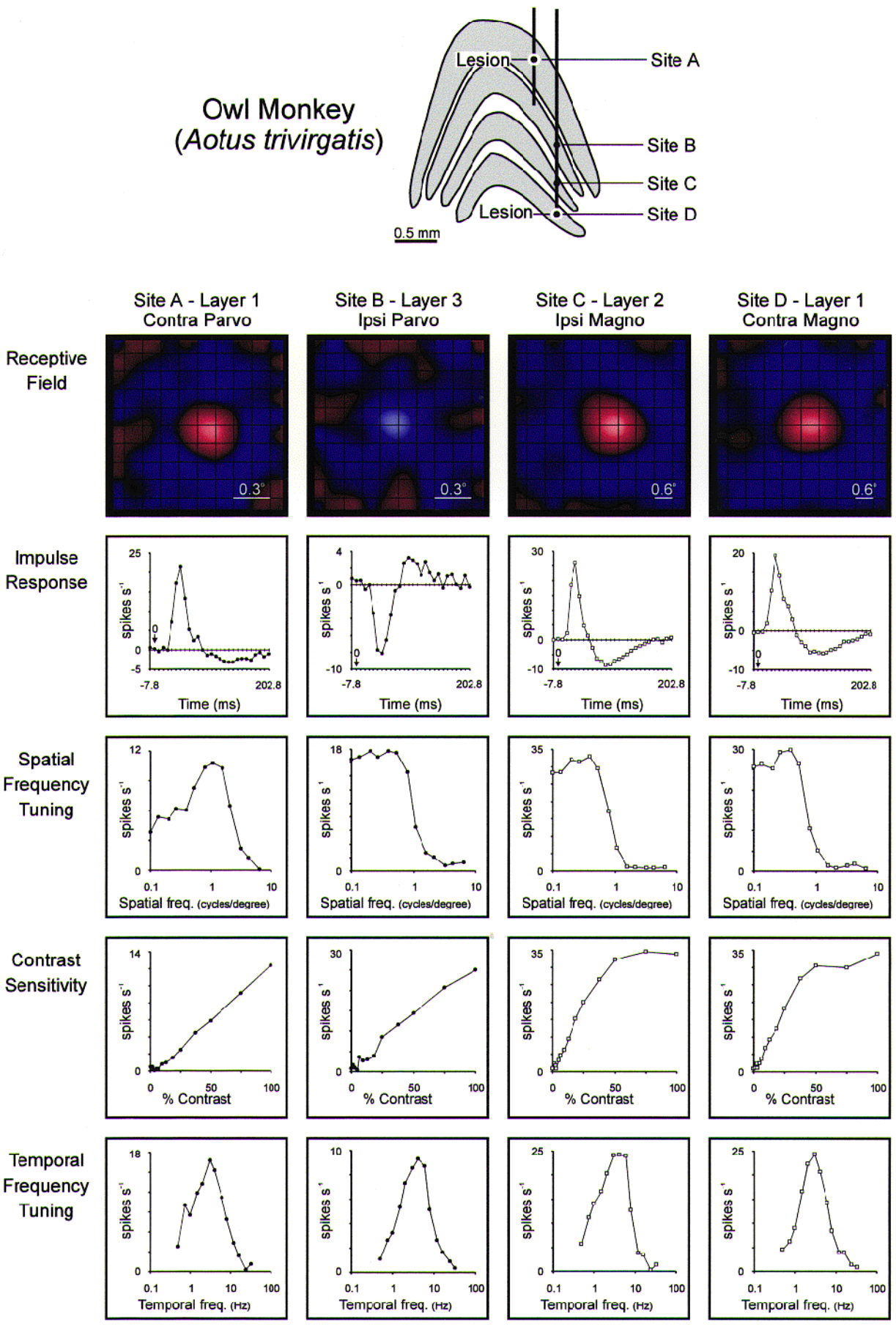
Owl Monkey
(Aotus trivirgatis)
Lesion
Site A
Site B
Site C
Site D
Lesion
0.5 mm
Site A - Layer 1
Contra Parvo
Site B - Layer 3
Ipsi Parvo
Site C - Layer 2
Ipsi Magno
Site D - Layer 1
Contra Magno
Receptive Field
0.3°
0.3°
0.6°
0.6°
Impulse Response
spikes s⁻¹
Time (ms)
-7.8
202.8
Spatial Frequency Tuning
Spatial freq. (cycles/degree)
Contrast Sensitivity
% Contrast
Temporal Frequency Tuning
Temporal freq. (Hz)

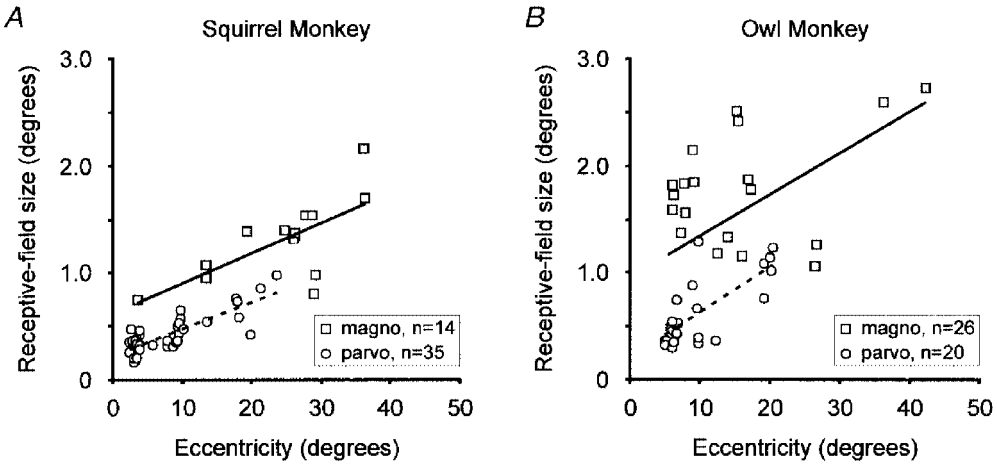

Figure 4. Receptive-field size (defined as 3·5σ, see Methods) varies with eccentricity and cell type (magnocellular *vs.* parvocellular)

In both squirrel monkey (*A*) and owl monkey (*B*) receptive-field size increases with eccentricity. At similar eccentricities, the receptive fields of magnocellular neurones (□, continuous line) are usually larger than those of parvocellular neurones (○, dashed line). For the population of magnocellular neurones in the squirrel monkey, the slope, y-intercept and correlation coefficient (r) values from the regression analysis were 0·028, 0·62 and 0·68, respectively. For parvocellular neurones in the squirrel monkey, the values were 0·025, 0·22 and 0·82, respectively. For the population of magnocellular neurones in the owl monkey, the slope, y-intercept and r values were 0·039, 0·95 and 0·53, respectively. For parvocellular neurones in the owl monkey, the values were 0·043, 0·20 and 0·53, respectively.

frequency tuning was characterized first, so that all subsequent tests could be performed with a near-optimal spatial frequency. Second, responses were measured at a range of contrasts. As in the macaque (Kaplan & Shapley, 1986), parvocellular responses had low gain and rarely saturated at high contrasts. Magnocellular neurones had high gain and usually showed a half-maximum response to gratings of approximately 20% contrast. Third, temporal tuning was tested at one or two different contrasts. When responses at 50% contrast were compared for both cell types, magnocellular neurones tended to have somewhat higher optimal frequencies, higher cutoffs, and more low-frequency attenuation. When the magnocellular cells were tested at 25% contrast, however, differences between magnocellular and parvocellular neurones were less pronounced. In the following sections, all of the points illustrated in Figs 2 and 3 are quantified for the entire population of cells studied.

Receptive-field size

We examined the size of receptive-field centres with respect to cell type (magnocellular *vs.* parvocellular) and eccentricity in both the squirrel monkey and owl monkey. The size of the receptive-field centre was determined by fitting the best single two-dimensional Gaussian to the spatial receptive field (the value reported is 3·5σ; see Methods). Our sample was not large enough to determine the form of the relation between eccentricity and receptive field size (for this analysis in the macaque see Croner & Kaplan, 1995). We therefore performed linear regression on each population of neurones (see Fig. 4 legend for fit parameters). For both magnocellular and parvocellular neurones in both the squirrel monkey and owl monkey, receptive-field centre size increased with eccentricity (Fig. 4). Comparison of cell types revealed that the centre size of magnocellular neurones was usually larger than that of parvocellular neurones at the same eccentricity (Fig. 4), on average by a factor of 1·5–3.

Time course and magnitude of visual responses

To facilitate comparison between cells, the time course and magnitude of visual responses were characterized with several parameters derived from the impulse responses. As illustrated in the schematic diagram in Fig. 5*A*, we calculated the time to peak response (t_{max}), the magnitude of the peak, and the transience.

In the macaque monkey, magnocellular neurones are known to have shorter latencies between stimulus and response than do parvocellular neurones (Maunsell *et al.* 1999). In both the squirrel monkey and owl monkey, we examined the latency (t_{max}) between stimulus onset and maximum response and similarly found shorter latencies for magnocellular neurones than for parvocellular neurones (Fig. 5*B*). Both magnocellular and parvocellular neurones in the squirrel monkey had shorter t_{max} values (mean values: 27·5 and

Figure 3. Examples of the response properties of neurones encountered during two adjacent electrode penetrations in the LGN of the owl monkey

All details as in Fig. 2.

34·9 ms, respectively) than either magnocellular or parvocellular neurones in the owl monkey (mean values: 40·4 and 48·8 ms, respectively).

The peak magnitude was taken as the integral of the impulse response before the rebound. In both the squirrel monkey and owl monkey, the impulse responses of magnocellular neurones had significantly larger peak magnitudes (mean values: 80·1 and 61·0 spikes s^{-1}, respectively) than those of parvocellular neurones (mean values: 23·6 and 19·4 spikes s^{-1}, respectively; Fig. 5*C*).

Although the rebound magnitude has no simple interpretation, it can be related to a more conventional measure – transience (Cleland *et al.* 1971; Ikeda & Wright, 1972; see Usrey *et al.* 1999) – in the following way. Transience is normally measured by recording the step response to a sustained stimulus. Because a sustained stimulus is the integral of an impulse stimulus, the step response for a linearly summating neurone should be the integral of the impulse response (see Usrey *et al.* 1999). The peak magnitude of the impulse response should therefore be equal to peak firing rate of the step response. The integral of the entire impulse response (or the peak magnitude minus the rebound magnitude, see Fig. 5*A*) should be equal to the plateau of the step response. By definition, a perfectly sustained step response would have a plateau equal to the peak, a perfectly transient step response would have a plateau of zero. Our measure of transience, rebound magnitude/peak magnitude, has exactly these properties. As might be expected (see Sherman *et al.* 1976), magnocellular neurones in both squirrel monkey and owl monkey were more transient (0·87 and 0·90, respectively) than parvocellular neurones (0·58 and 0·58; Fig. 5*D*).

Contrast gain and response saturation

The contrast gain of LGN neurones was measured using drifting (4 Hz) sinusoidal gratings of optimal spatial frequency and various levels of contrasts, from 1·5 to 100%. In both squirrel monkey (Fig. 6*A*) and owl monkey (Fig. 6*B*), magnocellular neurones were much more responsive to low contrast gratings than were parvocellular neurones. Furthermore, at any given contrast magnocellular neurones responded more vigorously than did parvocellular neurones. Magnocellular responses depended linearly on contrast up to 12–25%, but saturated at higher contrasts. Parvocellular neurones responded in a linear fashion up to 100% contrast.

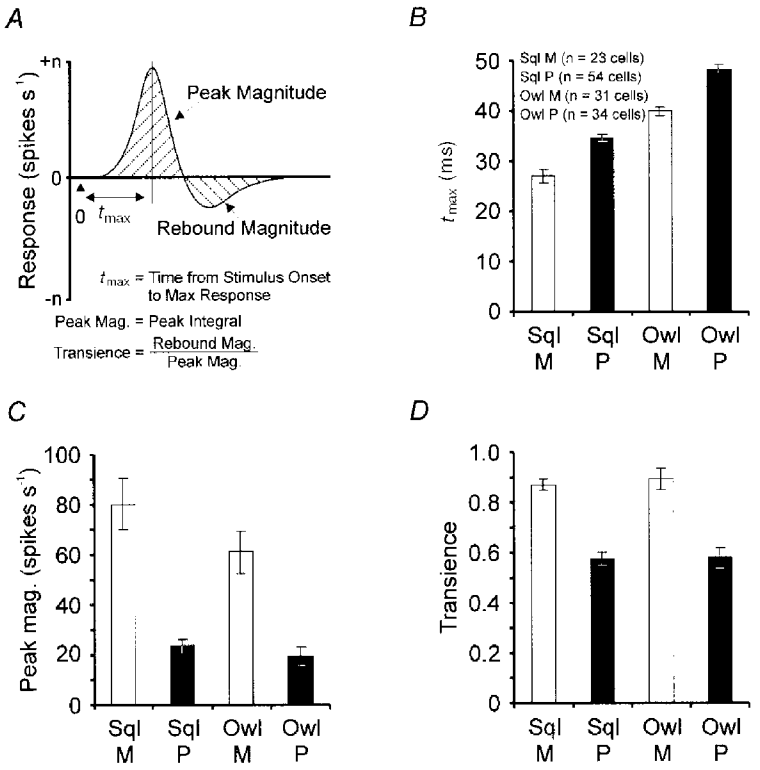

Figure 5. Comparison of the time course, magnitude and transience of visual responses of magnocellular and parvocellular neurones in the squirrel monkey and owl monkey

Impulse responses were calculated (see Methods) for each neurone in this study. *A*, impulse responses were used to quantify the time course, magnitude and transience of each neurone's response. *B*, in both squirrel (Sql) monkey and owl monkey, magnocellular (M) neurones had shorter latencies between stimulus onset and maximum response (t_{max}) than those of parvocellular (P) neurones. *C*, peak magnitude (mag.) of response was greater for magnocellular neurones than for parvocellular neurones in both squirrel monkey and owl monkey. *D*, transience of response was greater for magnocellular neurones than for parvocellular neurones in both squirrel monkey and owl monkey. In *B–D*, error bars indicate standard error of the mean.

Although LGN responses were usually more vigorous in the squirrel monkey than in the owl monkey, contrast–response curves looked similar when normalized for each cell's maximum response (Fig. 6*C*).

To quantify the difference in contrast–response curves, we performed two separate analyses. First we calculated contrast gain: the slope of each neurone's contrast–response curve (by linear regression) over the early, linear portion of the curve (1·5–12·5% contrast for magnocellular neurones; 1·5–25% contrast for parvocellular neurones). As expected, slopes were higher for magnocellular neurones than for parvocellular neurones in the squirrel monkey (1·35 ± 0·14 and 0·17 ± 0·03 spikes s^{-1} (% contrast)$^{-1}$, respectively) and in the owl monkey (0·57 ± 0·07 and 0·15 ± 0·04 spikes s^{-1} (% contrast)$^{-1}$, respectively).

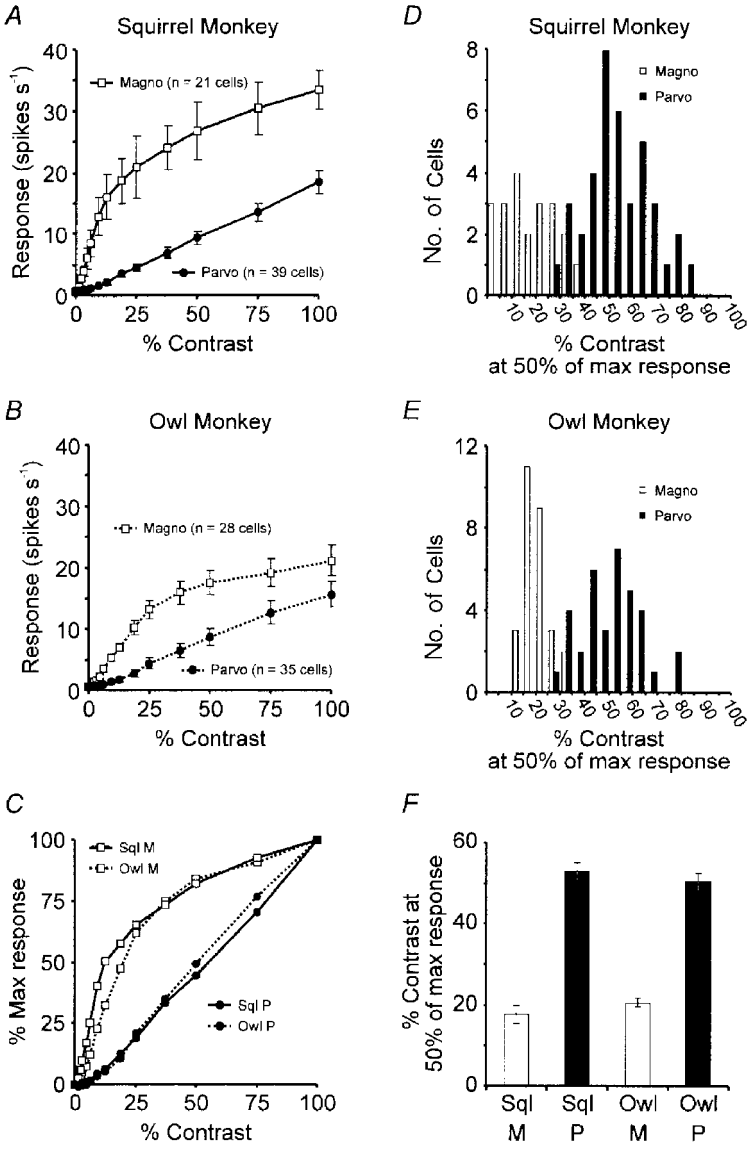

Figure 6. Contrast gain of LGN neurones

A and *B*, magnocellular and parvocellular responses to drifting sinusoidal gratings (4 Hz, optimal spatial frequency) of various contrasts (1·5—100%) are shown for the squirrel monkey (*A*) and owl monkey (*B*). Magnocellular neurones were much more responsive to low contrast gratings than were parvocellular neurones. Magnocellular responses begin to saturate at contrasts above 10–20%. Parvocellular neurones respond linearly to contrasts up to 100%. At any given contrast, owl monkey responses were less vigorous than squirrel monkey responses; response curves appear similar when normalized by each cell's maximum response (*C*). In both squirrel monkey (*D*) and owl monkey (*E*), the percentage contrast for evoking 50% of a cell's maximum response was less for magnocellular neurones than for parvocellular neurones. *F*, on average, the percentage contrast needed to evoke a half-maximal response in magnocellular neurones was 17·7% (squirrel monkey) and 20·5% (owl monkey); the percentage contrast required for parvocellular neurones was 52·9% (squirrel monkey) and 50·3% (owl monkey). Error bars in *A*, *B*, *C* and *F* indicate standard error of the mean.

Next, we determined the contrast needed to evoke 50% of each neurone's maximum response (as interpolated with a cubic spline). In both squirrel monkey (Fig. 6*D*) and owl monkey (Fig. 6*E*), there was almost no overlap in the distributions for magnocellular and parvocellular neurones. On average, magnocellular neurones required less contrast to evoke the half-maximal response (squirrel monkey, 17·7%; owl monkey, 20·5%) than did parvocellular neurones (squirrel monkey, 52·9%; owl monkey, 50·3%; Fig. 6*F*). Although our sample size was too small to address the question rigorously, these values did not depend significantly on the eccentricity of the receptive fields (for an analysis of this issue in the macaque see Croner & Kaplan, 1995).

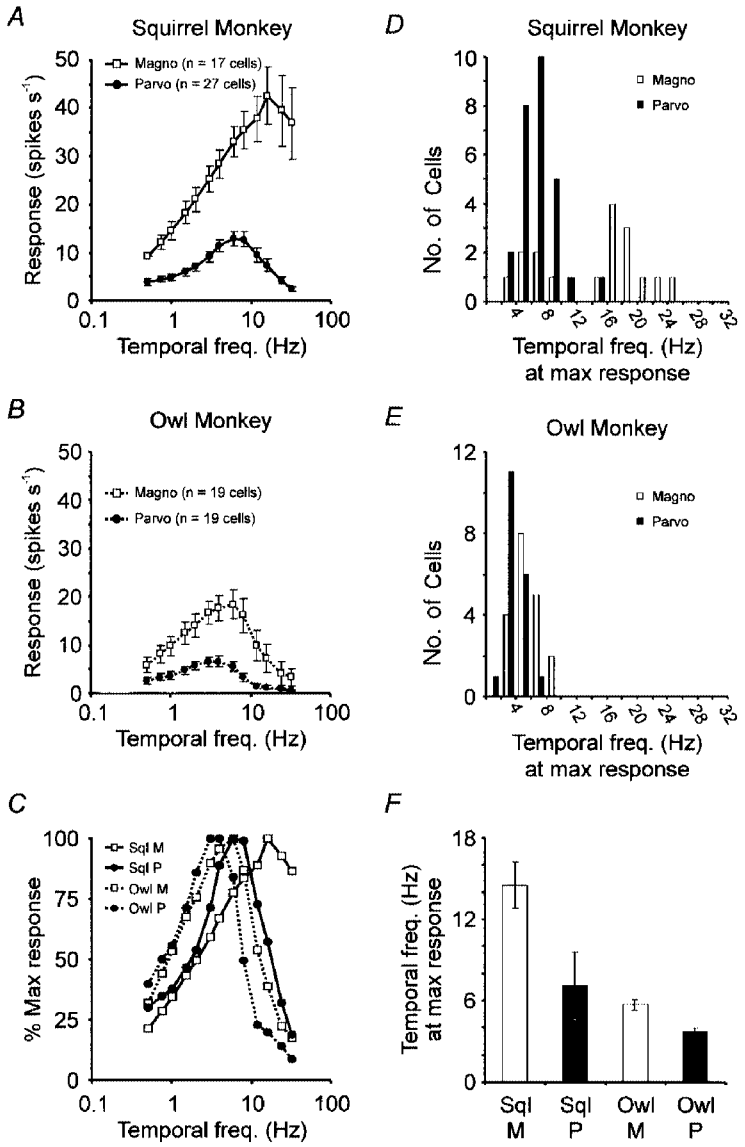

Figure 7. Temporal-frequency tuning of LGN neurones in the magnocellular and parvocellular layers of the LGN in the squirrel monkey and owl monkey

A and *B*, average responses of magnocellular and parvocellular neurones in the squirrel monkey (*A*) and owl monkey (*B*) to sinusoidal gratings (50% contrast, optimal spatial frequency) drifting at various temporal frequencies (freq., 0·5–32 Hz). Within the squirrel monkey and within the owl monkey, magnocellular neurones were much more responsive to rapidly drifting gratings than were parvocellular neurones. *C*, at any given temporal frequency, owl monkey responses were less vigorous than squirrel monkey responses. In both squirrel monkey (*D*) and owl monkey (*E*), the temporal frequency for evoking a maximum (max) response was greater for magnocellular neurones than for parvocellular neurones. *F*, in the squirrel monkey, the average temporal frequency of drifting gratings needed to evoke maximal response was 14·4 Hz for magnocellular neurones and 7·1 Hz for parvocellular neurones. In the owl monkey, the average temporal frequency for maximal response was 5·7 Hz for magnocellular neurones and 3·7 Hz for parvocellular neurones. Error bars in *A*, *B*, *C*, and *F* indicate standard error of the mean.

Temporal-frequency tuning

Temporal-frequency tuning was assessed by drifting sinusoidal gratings of near-optimal spatial frequency and 50% contrast past each cell's receptive field at various temporal frequencies (from 0·5 to 32 Hz, occasionally as high as 64 Hz for some magnocellular neurones). Average temporal frequency–response curves from squirrel monkey and owl monkey are shown in Figs 7*A–C*. In the squirrel monkey, magnocellular neurones were much more responsive than were parvocellular neurones to stimuli drifting at high rates. At 50% contrast, magnocellular neurones in squirrel monkey responded strongly to drifting gratings at 32 Hz, while parvocellular neurones were virtually unresponsive. Although all responses in the owl monkey were shifted to lower frequencies, magnocellular neurones were more responsive at higher frequencies (e.g. 12 Hz) than parvocellular neurones.

In both squirrel monkey and owl monkey, we determined the temporal frequency that would produce a maximum response by interpolating (with a cubic spline) the temporal frequency–response curves for each neurone. For squirrel monkeys, the distribution for magnocellular and parvocellular neurones was partially overlapping (Fig. 7*D*), although most magnocellular neurones preferred temporal frequencies much higher than that preferred by parvocellular neurones. For owl monkeys, the distributions were almost completely overlapping (Fig. 7*E*). The average temporal frequency for maximum response in the squirrel monkey was 14·4 Hz for magnocellular neurones and 7·1 Hz for parvocellular neurones (Fig. 7*F*). In the owl monkey, the average preferred frequency was 5·7 Hz for magnocellular neurones and 3·7 Hz for parvocellular neurones (Fig. 7*F*). As with contrast gain, these values did not appear to depend significantly on the eccentricity of the receptive fields.

Contrast gain control in magnocellular neurones

Although a significant difference in temporal tuning was seen between magnocellular and parvocellular neurones of both species, part of this difference was contrast dependent. In the analysis above, temporal tuning of magnocellular and parvocellular neurones was compared at 50% contrast, well into the saturating range of magnocellular neurones. For some magnocellular neurones (11 in the squirrel monkey, 4 in the owl monkey), temporal tuning was measured at both

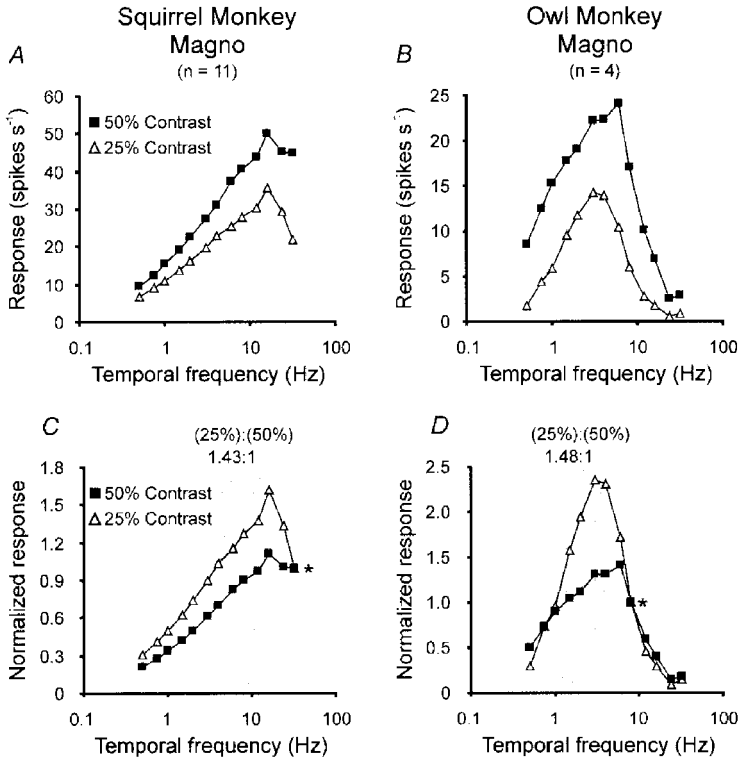

Figure 8. Magnocellular neurones in both squirrel monkey and owl monkey display a contrast gain control mechanism

A and *B*, temporal frequency–response curves for magnocellular neurones in the squirrel monkey and owl monkey. Separate response curves are shown for responses to drifting sinusoidal gratings of 50% contrast and 25% contrast. At all temporal frequencies tested (0·5–32 Hz), responses (spikes s^{-1}) to 50% contrast gratings were greater than those to 25% contrast gratings. However, compared with responses at 25% contrast, responses at 50% contrast were relatively attenuated at frequencies below the optimal (better appreciated in *C* and *D*). *C* and *D*, response curves normalized by responses to rapidly drifting gratings (indicated by the asterisks, 32 Hz for squirrel monkey and 8 Hz for owl monkey). Responses at 50% contrast are relatively attenuated at lower frequencies compared with those at 25% contrast.

25 and 50% contrast, as illustrated in Fig. 2. Compared with the responses at 25% contrast, responses at 50% contrast were relatively stronger at frequencies above the optimal and attenuated at frequencies below the optimal. These effects were quite consistent, as illustrated in the averaged temporal-frequency tuning curves for the squirrel monkey (Fig. 8*A*) and the owl monkey (Fig. 8*B*). To facilitate comparison, the average tuning curve at each contrast was normalized to its value at a high frequency (roughly twice the optimal, or 32 Hz for the squirrel monkey and 8 Hz for the owl monkey; Figs 8*C* and *D*). Consistently, the responses at 50% contrast are relatively attenuated at lower frequencies. To quantify the difference between the high- and low-contrast curves, we summed the normalized responses at a range of lower frequencies: 4–16 Hz for squirrel monkey, 1–4 Hz for owl monkey. For the squirrel monkey, the relative responses at the low frequencies were 1·43 times greater at 25% than at 50% contrast. For the owl monkey, this ratio was 1·48. These ratios are for the averaged responses over all cells, but the effect was consistently seen for most individual cells (ratio $>1{\cdot}3$ for 8 of 11 magnocellular cells in the squirrel monkey, 4 of 4 in the owl monkey). The ranges of frequencies used in these comparisons, although arbitrary, were chosen because they showed the effect quite strongly and because responses at lower frequencies were often weak and relatively noisy.

This contrast-dependent shift in temporal-frequency tuning is probably the result of the retinal contrast gain control, first described in the cat (Shapley & Victor, 1978). In primates, the contrast gain control has been seen in some magnocellular-projecting cells in the macaque retina (Benardete *et al.* 1992; Benardete & Kaplan, 1999) and marmoset retina (Yeh *et al.* 1995), as well as in magnocellular neurones of the marmoset LGN (Kremers *et al.* 1997). It should be noted that the contrasts considered in the present study (25% *versus* 50%) were much higher than those typically used to study the contrast gain control (e.g. $\leqslant$12%, in Benardete & Kaplan, 1999).

Surround attenuation

The strength of a neurone's receptive-field surround was assessed by comparing neuronal responses to gratings of optimal spatial frequency (which modulates the centre, but not the surround) with responses to gratings of low spatial frequency (which drives both centre and surround antagonistically) (see Fig. 9*A*). To compare receptive fields of different sizes, we took the ratio of the response at the optimal frequency to responses at either $\frac{1}{2}$ or $\frac{1}{4}$ the optimal frequency (we did not make difference-of-Gaussian fits because low-frequency responses were sometimes poorly sampled, especially for the largest receptive fields, and thus the fits were prone to error). Although there was a small number of cells with very little surround attenuation (see Figs 2 and 3), the average responses were quite consistent. For all populations of cells, magnocellular and parvocellular in both the squirrel monkey and owl monkey, neuronal responses were attenuated by approximately 25% when using gratings of $\frac{1}{2}$ the peak spatial frequency and by approximately 40–50% when using gratings of $\frac{1}{4}$ the peak spatial frequency (Figs 9*B* and *C*). By this measure, therefore, there was little difference between the populations in terms of strength of the surround.

Spatial summation

Finally, linearity of spatial summation was assessed with a modified null test (Enroth-Cugell & Robson, 1966;

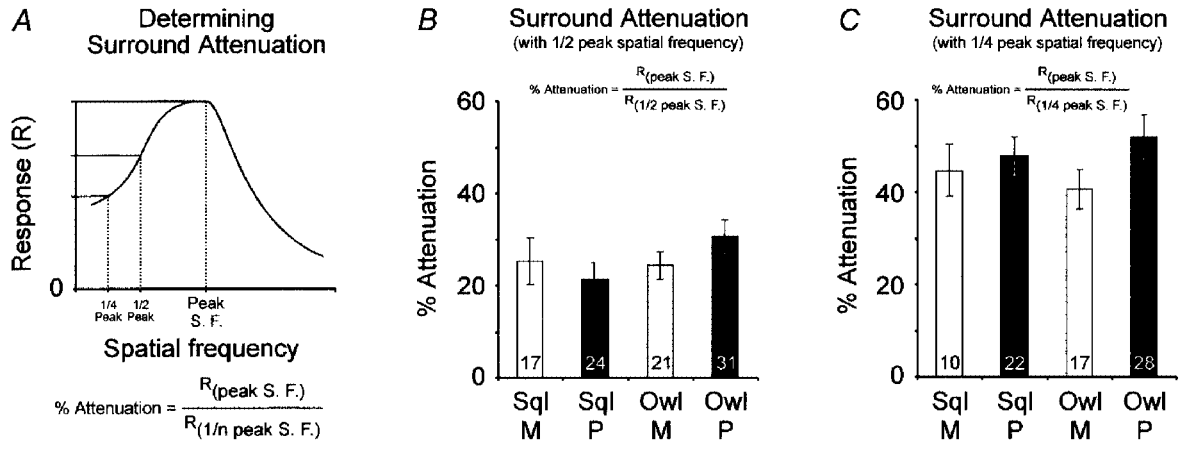

Figure 9. Strength of receptive-field surround is similar for magnocellular and parvocellular neurones in the squirrel monkey and owl monkey

A, sinusoidal gratings of optimal spatial frequency (the spatial frequency that maximally drives receptive field centres) and $\frac{1}{2}$ and $\frac{1}{4}$ the optimal spatial frequency (frequencies that modulate centres and surrounds antagonistically) were used to examine the strength of receptive-field surrounds (see text). *B*, sinusoidal gratings with spatial frequencies $\frac{1}{2}$ the peak spatial frequency attenuated peak responses by ~25%. *C*, sine-wave gratings with spatial frequencies $\frac{1}{4}$ of the peak attenuated peak responses by ~50%. Error bars in *B* and *C* indicate standard error of the mean.

Hochstein & Shapley, 1976; see Methods). For all cells tested (squirrel monkey: 18 magno- and 27 parvocellular neurones; owl monkey: 19 magno- and 31 parvocellular neurones; data not shown), spatial summation was linear, that is, Y cells were not observed in either species. By comparison, some studies of the macaque LGN have found that 25% of magnocellular neurones were Y cells (Kaplan & Shapley, 1982; Blakemore & Vital-Durand, 1986), although another study reported only 5% (Derrington & Lennie, 1984). While the difference may reflect a fundamental difference between the species, it is also possible that our sample of magnocellular neurones was too small to detect a sparse population of Y cells.

DISCUSSION

We studied the visual responses of geniculate neurones in two species of New World primates – the diurnal squirrel monkey and the nocturnal owl monkey. In both species, magnocellular and parvocellular neurones were compared in terms of five different parameters: (1) receptive-field size, (2) strength and time course of their responses to white-noise stimuli (impulse responses), (3) contrast gain of responses to sinusoidal gratings, (4) temporal-frequency tuning, and (5) spatial frequency tuning. For each of these categories, magnocellular and parvocellular neurones paralleled the differences previously described in macaque (De Valois, 1960; Wiesel & Hubel, 1966; Gouras, 1968; De Monasterio & Gouras, 1975; Schiller & Malpeli, 1978, Kaplan & Shapley, 1982, 1986; Derrington & Lennie, 1984; Derrington *et al.* 1984; Maunsell *et al.* 1999; reviewed in Lee, 1996), marmoset (Yeh *et al.* 1995; Kremers & Weiss, 1997; Kremers *et al.* 1997; Martin *et al.* 1997; White *et al.* 1998; Solomon *et al.* 1999), and galago (Norton & Casagrande, 1982; Norton *et al.* 1988). Compared with parvocellular neurones, magnocellular neurones in both the squirrel monkey and owl monkey had the following properties. (1) Their receptive fields were usually larger. (2) Their impulse responses were higher in magnitude, faster to reach their peak response, and were more transient (as measured by the relative amplitude of the rebound). (3) Their contrast gains were greater and their responses saturated at high contrasts. Half-maximal responses for magnocellular neurones were found at ∼20% contrast, compared with ∼50% for parvocellular neurones. (4) Their responses to high temporal frequencies were stronger, although there was considerable overlap between the two categories. (5) The strength of their surrounds, as measured by response attenuation at low spatial frequencies, was on average equal. Finally, as seen in the macaque (Benardete *et al.* 1992; Benardete & Kaplan, 1999) and marmoset (Yeh *et al.* 1995; Kremers *et al.* 1997), magnocellular neurones showed evidence of a contrast gain-control mechanism (Shapley & Victor, 1978).

Although the relative differences between magnocellular and parvocellular neurones were seen in both the squirrel monkey and owl monkey, there were several distinct differences between the species. First, the temporal response properties, particularly the time to peak response (Fig. 5) and the optimal temporal frequency (Fig. 7), were relatively slower in the owl monkey. Second, all responses in the owl monkey, even to optimal stimuli, were less vigorous.

These two findings – that the owl monkey has both slower response dynamics and lower peak firing rates – may be related. That is, if responses are slow, then encoding of these responses is possible with a low spike rate. Alternatively, if responses are faster, as in the squirrel monkey, higher response rates are required in order to encode these rapidly varying signals.

The parvocellular pathway and colour vision

There are strong similarities between the magnocellular and parvocellular pathways in the LGNs in New World and Old World monkeys (reviewed in Casagrande & Kaas, 1994). Both diurnal and nocturnal New World monkeys (*Cebus*, in the same family, and *Aotus*) have been shown to have M and P cell types in the retina, similar to those seen in the macaque (Silveira *et al.* 1994). These cells project respectively to the ventral two magnocellular layers and to the dorsal parvocellular layers of the LGN. As in the macaque, neurones in the magnocellular and parvocellular LGN project to the upper and lower tiers of layer 4C, respectively.

Several striking differences, however, are found between the visual systems of the macaque and either the owl monkey or the squirrel monkey. The macaque is a diurnal trichromat, with a highly developed red/green opponent system. Male squirrel monkeys (although not all females; Jacobs & Neitz, 1985) are dichromats and thus lack any red/green opponent responses. Owl monkeys are nocturnal monochromats (Jacobs, 1977; Jacobs *et al.* 1993). Thus it might be expected that the parvocellular system in particular could be significantly different between the three species. Instead, we have found that parvocellular cells in both New World species are grossly similar to each other and to the macaque. This result is consistent with past work in the owl monkey (O'Keefe *et al.* 1998), marmoset (Yeh *et al.* 1995; Kremers & Weiss, 1997; Kremers *et al.* 1997; White *et al.* 1998: Solomon *et al.* 1999) and galago (Norton & Casagrande, 1982; Norton *et al.* 1988). One slight difference between the species is that no Y cells were observed in the magnocellular LGN of either the squirrel monkey or the owl monkey.

Two roles have been proposed for parvocellular neurones in the macaque visual system. The first is that they might subserve the discrimination of the finest spatial detail (reviewed in Schiller & Logothetis, 1990; Merigan & Maunsell, 1993). The second is that they are the basis of red/green colour vision (reviewed in Lee, 1996; but see Lennie *et al.* 1991; Rodieck, 1991). Clearly this second role cannot be played by parvocellular neurones in either the squirrel monkey (males) or owl monkey. In other respects, however, the physiology of parvocellular neurones is similar between

the three species (see also White *et al.* 1998). While these findings do not preclude a role for parvocellular neurones in red/green vision in the macaque, they argue that parvocellular neurones play an important role in achromatic vision, both at the finest spatial scale and perhaps in the discrimination among moderate levels of contrast.

Benardete, E. A. & Kaplan, E. (1999). The dynamics of primate M retinal ganglion cells. *Visual Neuroscience* **16**, 355–368.

Benardete, E. A., Kaplan, E. & Knight, B. W. (1992). Contrast gain control in the primate retina: P cells are not X-like, some M cells are. *Visual Neuroscience* **8**, 483–486.

Blakemore, C. & Vital-Durand, F. (1986). Organization and post-natal development of the monkey's lateral geniculate nucleus. *Journal of Physiology* **380**, 453–491.

Casagrande, V. A. (1994). A third parallel pathway to primate area V1. *Trends in Neurosciences* **17**, 305–310.

Casagrande, V. A. & Kaas, J. H. (1994). The afferent, intrinsic, and efferent connections of primary visual cortex in primates. In *Cerebral Cortex. Primary Visual Cortex in Primates*, vol. 10, ed. Peters, A. & Rockland, K. S., pp. 201–259. Plenum Press, New York.

Cleland, B. G., Dubin, M. W. & Levick, W. R. (1971). Sustained and transient neurones in the cat's retina and lateral geniculate nucleus. *Journal of Physiology* **217**, 473–496.

Croner, L. J. & Kaplan, E. (1995). Receptive fields of P and M ganglion cells across the primate retina. *Vision Research* **35**, 7–24.

De Monasterio, F. M. & Gouras, P. (1975). Functional properties of ganglion cells of the rhesus monkey retina. *Journal of Physiology* **251**, 167–195.

Derrington, A. M., Krauskopf, J. & Lennie, P. (1984). Chromatic mechanisms in lateral geniculate nucleus of macaque. *Journal of Physiology* **357**, 241–265.

Derrington, A. M. & Lennie, P. (1984). Spatial and temporal contrast sensitivities of neurones in lateral geniculate nucleus of macaque. *Journal of Physiology* **357**, 219–240.

De Valois, R. L. (1960). Color vision mechanisms in the monkey. *Journal of General Physiology* **43**, 115–128.

Diamond, I. T., Conley, M., Itoh, K. & Fitzpatrick, D. (1985). Laminar organization of geniculocortical projections in *Galago senegalensis* and *Aotus trivirgatus*. *Journal of Comparative Neurology* **242**, 584–610.

Doty, R. W., Glickstein, M. & Calvin, W. H. (1966). Lamination of the lateral geniculate nucleus in the squirrel monkey, *Saimiri sciureus*. *Journal of Comparative Neurology* **127**, 335–340.

Enroth-Cugell, C. & Robson, J. G. (1966). The contrast sensitivity of retinal ganglion cells of the cat. *Journal of Physiology* **187**, 517–552.

Fitzpatrick, D., Itoh, K. & Diamond, I. T. (1983). The laminar organization of the lateral geniculate body and the striate cortex in the squirrel monkey (*Saimiri sciureus*). *Journal of Neuroscience* **3**, 673–702.

Gouras, P. (1968). Identification of cone mechanisms in monkey ganglion cells. *Journal of Physiology* **199**, 533–547.

Hawken, M. J., Shapley, R. M. & Grosof, D. H. (1996). Temporal-frequency selectivity in monkey visual cortex. *Visual Neuroscience* **13**, 477–492.

Hendry, S. H. C. & Reid, R. C. (2000). The koniocellular pathway in primate vision. *Annual Review of Neuroscience* (in the Press).

Hochstein, S. & Shapley, R. M. (1976). Quantitative analysis of retinal ganglion cell classifications. *Journal of Physiology* **262**, 237–264.

Ikeda, H. & Wright, M. J. (1972). Receptive field organization of 'sustained' and 'transient' retinal ganglion cells which subserve different function roles. *Journal of Physiology* **227**, 769–800.

Jacobs, G. H. (1977). Visual capacities of the owl monkey (*Aotus trivirgatus*). I. Spectral sensitivity and color vision. *Vision Research* **17**, 811–820.

Jacobs, G. H. (1984). Differences in spectral response properties of LGN cells in male and female squirrel monkeys. *Vision Research* **23**, 461–468.

Jacobs, G. H., Deegan, J. F., Deegan, D., Neitz, J., Crognale, M. A. & Neitz, M. (1993). Photopigments and color vision in the nocturnal monkey, Aotus. *Journal of Comparative Neurology* **33**, 1773–1783.

Jacobs, G. H. & De Valois, R. L. (1965). Chromatic opponent cells in squirrel monkey lateral geniculate nucleus. *Nature* **206**, 487–489.

Jacobs, G. H. & Neitz, J. (1985). Color vision in squirrel monkeys: sex-related differences suggest the mode of inheritance. *Vision Research* **25**, 141–143.

Jones, A. E. (1966). The lateral geniculate complex of the owl monkey *Aotus trivirgatus*. *Journal of Comparative Neurology* **126**, 171–179.

Kaas, J. H., Guillery, R. W. & Allman, J. M. (1972). Some principles of organization in the dorsal lateral geniculate nucleus. *Brain, Behavior and Evolution* **6**, 253–299.

Kaas, J. H., Huerta, M. F., Weber, J. T. & Harting, J. K. (1978). Patterns of retinal terminations and laminar organization of the lateral geniculate nucleus of primates. *Journal of Comparative Neurology* **182**, 517–553.

Kaplan, E. & Shapley, R. M. (1982). X and Y cells in the lateral geniculate nucleus of macaque monkeys. *Journal of Physiology* **330**, 125–143.

Kaplan, E. & Shapley, R. M. (1986). The primate retina contains two types of ganglion cells, with high and low contrast sensitivity. *Proceedings of the National Academy of Sciences of the USA* **83**, 2755–2757.

Kremers, J. & Weiss, S. (1997). Receptive field dimensions of lateral geniculate cells in the common marmoset (Callitrhix jacchus). *Journal of Comparative Neurology* **37**, 2171–2181.

Kremers, J., Weiss, S. & Zrenner, E. (1997). Temporal properties of marmoset lateral geniculate cells. *Journal of Comparative Neurology* **37**, 2649–2660.

Lee, B. B. (1996). Receptive field structure in the primate retina. *Journal of Comparative Neurology* **36**, 631–644.

Lennie, P., Haake, P. W. & Williams, D. R. (1991). The design of chromatically opponent receptive fields. In *Computational Models of Visual Processing*, ed. Landy, M. S. & Movshon, J. A., pp. 71–82. MIT Press, Cambridge, MA, USA.

Martin, P. R., White, A. J., Goodchild, A. K., Wilder, H. D. & Sefton, A. E. (1997). Evidence that blue-on cells are part of the third geniculocortical pathway in primates. *European Journal of Neuroscience* **9**, 1536–1541.

Maunsell, J. H. R., Ghose, G. M., Assad, J. A., McAdams, C. J., Boudreau, C. E. & Noerager, B. D. (1999). Visual response latencies of magnocellular and parvocellular LGN neurons in macaque monkeys. *Visual Neuroscience* **16**, 1–14.

Merigan, W. H. & Maunsell, J. H. (1993). How parallel are the primate visual pathways? *Annual Review of Neuroscience* **16**, 369–402.

Norton, T. T. & Casagrande, V. A. (1982). Laminar organization of receptive-field properties in lateral geniculate nucleus of bush baby (*Galago crassicaudatus*). *Journal of Neurophysiology* **47**, 715–741.

Norton, T. T., Casagrande, V. A., Irvin, G. E., Sesma, M. A. & Petry, H. M. (1988). Contrast-sensitivity functions of W-, X-, and Y-like relay cells in the lateral geniculate nucleus of bush baby, *Galago crassicaudatus*. *Journal of Neurophysiology* **59**, 1639–1656.

O'Keefe, L. P., Levitt, J. B., Kiper, D. C., Shapley, R. M. & Movshon, J. A. (1998). Functional organization of owl monkey lateral geniculate nucleus and visual cortex. *Journal of Neurophysiology* **80**, 594–609.

Reid, R. C. & Shapley, R. M. (1992). Spatial structure of cone inputs to receptive fields in primate lateral geniculate nucleus. *Nature* **356**, 716–718.

Reid, R. C., Victor, J. D. & Shapley, R. M. (1997). The use of m-sequences in the analysis of visual neurons: Linear receptive field properties. *Visual Neuroscience* **16**, 1015–1027.

Rodieck, R. W. (1991). Which cells code for color? In *From Pigments to Perception*, ed. Valberg, A. & Lee, B. B, pp. 83–93. Plenum Press, New York.

Schiller, P. H. & Logothetis, N. K. (1990). The color-opponent and broad-band channels of the primate visual system. *Trends in Neurosciences* **13**, 392–398.

Schiller, P. H. & Malpeli, J. G. (1978). Functional specificity of lateral geniculate nucleus laminae of the rhesus monkey. *Journal of Neurophysiology* **41**, 788–797.

Shapley, R. M. (1992). Parallel retinocortical channels: X and Y and P and M. In *Applications of Parallel Processing in Vision*, ed. Brannan, J., pp. 3–36. Elsevier Science Publishers, New York.

Shapley, R. M. & Victor, J. D. (1978). The effect of contrast on the transfer properties of cat retinal ganglion cells. *Journal of Physiology* **285**, 275–298.

Sherman, S. M., Wilson, J. R., Kaas, J. H. & Webb, S. V. (1976). X- and Y-cells in the dorsal lateral geniculate nucleus of the owl monkey (*Aotus trivirgatus*). *Science* **192**, 475–477.

Silveira, L. C., Yamada, E. S., Perry, V. H. & Picanco-Diniz, C. W. (1994). M and P retinal ganglion cells of diurnal and nocturnal New-World monkeys. *NeuroReport* **5**, 2077–2081.

Solomon, S. G., White, A. J. & Martin, P. R. (1999). Temporal contrast sensitivity in the lateral geniculate nucleus of a New World monkey, the marmoset *Callithrix jacchus*. *Journal of Physiology* **517**, 907–917.

Sutter, E. E. (1992). A deterministic approach to nonlinear systems analysis. In *Nonlinear Vision: Determination of Neural Receptive Fields, Function, and Networks*. ed. Pinter, R. & Nabet, B., pp. 171–220. CRC Press, Cleveland, Ohio.

Usrey, W. M., Reppas, J. B. & Reid, R. C. (1999). Specificity and strength of retinogeniculate connections. *Journal of Neurophysiology* **82**, 3527–3540.

White, A. J., Wilder, H. D., Goodchild, A. K., Sefton, A. J. & Martin, P. R. (1998). Segregation of receptive field properties in the lateral geniculate nucleus of a New-World monkey, the marmoset Callithrix jacchus. *Journal of Neurophysiology* **80**, 2063–2076.

Wiesel, T. N. & Hubel, D. H. (1966). Spatial and chromatic interactions in the lateral geniculate body of the rhesus monkey. *Journal of Neurophysiology* **29**, 1115–1156.

Yeh, T., Lee, B. B., Kremers, J., Cowing, J. A., Hunt, D. M., Martin, P. R. & Troy, J. B. (1995). Visual responses in the lateral geniculate nucleus of dichromatic and trichromatic marmosets (*Callithrix jacchus*). *Journal of Neuroscience* **15**, 7892–7904.

Acknowledgements

This work was supported by NIH grants EY06604, EY10115, EY12196 and the Harvard Mahoney Neuroscience Institute. We thank Christine Couture for expert technical assistance, Sergey Yurgenson for computer programming, Adam Carter for participating in the owl monkey experiments, and John Assad, Michael Hawken, Margaret Livingstone and John Reppas for insightful comments on this manuscript.

Corresponding author

R. C. Reid: Department of Neurobiology, Harvard Medical School, 220 Longwood Avenue, Boston, MA 02115, USA.

Email: clay_reid@hms.harvard.edu

Author's present address

W. M. Usrey: University of California, Davis, 1544 Newton Court, Davis, CA 95616, USA.